The CXCR3 Binding Chemokine IP-10/CXCL10: Structure and Receptor Interactions†

Valerie Booth,‡ David W. Keizer,‡ Monique B. Kamphuis,‡ Ian Clark-Lewis,§ and Brian D. Sykes*,‡

Protein Engineering Network of Centres of Excellence and Department of Biochemistry, 713 Heritage Medical Research Center, University of Alberta, Edmonton, Alberta, Canada, T6G 2S2, and Biomedical Research Centre and Department of Biochemistry and Molecular Biology, University of British Columbia, Vancouver, British Columbia, Canada, V6T 1Z3

Received April 25, 2002; Revised Manuscript Received June 7, 2002

ABSTRACT: The structure of IP-10 was solved by NMR spectroscopy and represents the first structure from the class of agonists toward the receptor CXCR3. CXCR3 binding chemokines are unique in their ability to bind receptors from both the CC and CXC classes of chemokine receptors. An unusual structural feature of IP-10 was identified that may provide the basis for the ability of IP-10 to bind both CXCR3 and CCR3. The surface of IP-10 that interacts with the N-terminus of CXCR3 was defined by monitoring changes in the NMR spectrum of IP-10 upon addition of a CXCR3 N-terminal peptide. These studies indicated that the interaction involves a hydrophobic cleft, formed by the N-loop and 40s-loop region of IP-10, similar to the interaction surface observed for other chemokines such as IL-8. An additional region of interaction was observed that consists of a hydrophobic cleft formed by the N-terminus of IP-10 and 30s-loop of IP-10.

IP-10 (CXCL10) is a member of the chemokine family of small secretory proteins involved in immune and inflammatory responses. Chemokines play a key role in these processes by promoting recruitment and activation of different subpopulations of leukocytes (*1*). They fall into two main subfamilies based on the arrangement of the first two of four conserved cysteines, adjacent in CC chemokines and separated by one amino acid in CXC chemokines (*2*). Chemokines exert their effects by interacting with an appropriate seven-transmembrane G protein-coupled receptor on the surface of a leukocyte (*3*). Knowledge of the structural basis for the interaction of chemokines with their receptors is of significant importance to understanding chemokine function and to the design of therapeutic interventions for a number of pathologies that involve chemokines (*4*).

The receptors follow a similar nomenclature to the chemokines, with CC receptors interacting with CC chemokines and CXC receptors with CXC chemokines. IP-10 binds to and activates the receptor CXCR3, as do ITAC (CXCL11) and Mig (CXCL9) (*5*). Recently BCA-1 (CXCL13) (*6*) has been reported to also bind CXCR3 in addition to its previously known partner, CXCR5. Interestingly, while ITAC, IP-10, and Mig are agonists for CXCR3, they can also act as antagonists for CCR3 (*7*). The observation that certain chemokines can bind and activate one receptor, while binding and attenuating the activity of another receptor gives an indication of the complexity of the chemokine network. Elucidating the structural features that give rise to this ability would certainly aid in understanding how chemokines function.

Much of the investigation of CXC chemokines has focused on those that bind to neutrophils through the CXCR1 and CXCR2 receptors, as well as those that bind to CXCR4, an HIV-1 co-receptor. CXCR3 binding chemokines appear to act in a different way from CXCR1, 2, and 4, as they do not interact with neutrophils but act exclusively on activated T lymphocytes (type 1 T-helper cells) (*8*). This suggests that IP-10, ITAC, and Mig are involved in selective recruitment of effector T cells.

IP-10 is induced mainly by interferon γ (*9*, *10*), a cytokine typically associated with Th1 responses, and is secreted by a number of different cell types (*11*). IP-10 and Mig are highly expressed in several inflammatory skin conditions (*12*). Both IP-10 and CXCR3 are implicated in inflammation of the central nervous system of patients with multiple sclerosis and have been found to be upregulated in the brains of these patients (*13*, *14*). IP-10 and Mig are antiangiogenic (*15*, *16*) in contrast to other CXC chemokines, such as IL-8, that promote angiogenesis. Donor-derived IP-10 apparently plays a pivotal role in acute allograft rejection (*17*). Additionally, CXCR3 binding chemokines are expressed in the thymus and appear to play a role in lymphopoesis by controlling the transmigration of different subsets of mature thymocytes (*18*). Little is known about how distinct or overlapping the functional roles of IP-10, Mig, and ITAC are, but ITAC appears to be the most potent of the three (*19*, *20*).

† This work was supported by the Protein Engineering Network of Centres of Excellence. Additionally, V.B. is supported by fellowships from Canadian Institutes of Health Research (CIHR) and the Alberta Heritage Fund for Medical Research (AHFMR). M.K. acknowledges funding from Stichting Jo Kolk Studiefonds. We would like to acknowledge the Canadian National High Field NMR Centre (NANUC) for their assistance and use of the facilities. Operation of NANUC is funded by CIHR, the Natural Science and Engineering Research Council of Canada (NSERC) and the University of Alberta.

* Corresponding author.
‡ University of Alberta.
§ University of British Columbia.

10.1021/bi026020q CCC: $22.00
Published on Web 07/23/2002

Although there are many indications that CXCR3 binding chemokines play important roles in normal physiology as well as in several diseases, their function is just beginning to be elucidated. In particular, there were no structures solved for any CXCR3 binding chemokine before this study. To better understand how these proteins function and to provide a structural framework for the interpretation of other studies, we determined the NMR structure of IP-10. In addition, we investigated the characteristics of IP-10/receptor binding using a CXCR3 derived peptide.

MATERIALS AND METHODS

Sample Preparation. IP-10 and CXCR3 peptide were synthesized by stepwise solid-phase methods using *t*-butoxycarbonyl protection chemistry. After hydrogen fluoride deprotection, the polypeptide was folded and purified by reverse-phase HPLC as described previously (*21*). A mutant, monomeric form of IP-10 was also synthesized (NMeLeu 27) in which the amide proton of leucine 27 was replaced with a methyl group. The samples were lyophilized and stored at 4 °C.

Determination of the Association State of IP-10. Analytical ultracentrifugation was performed with wild-type IP-10 at 30 °C on a Beckman XL-1 instrument equipped with an AN50T1 rotor. IP-10 was dissolved at a concentration of ~0.7 mM in 20 mM sodium acetate, 100 mM NaCl, 1 mM NaN_3, pH 5.0. Data were recorded at four different rotor speeds and analyzed as described previously (*22*).

^{1}H-T_2 NMR relaxation times were measured with buffer conditions identical to those used in structure determination (2 mM IP-10, 1 mM DSS, 1 mM sodium azide, 90% H_2O/10% D_2O, pH 5.0) on a Varian Unity 600 MHz spectrometer at 20, 30, and 40 °C for wild-type IP-10 and on a Varian Inova 500 MHz spectrometer at 30 °C for the NMeLeu 27 mutant. A jump and return spin−echo pulse sequence (*23*, *24*) was used in order to remove *J* modulation from the T_2 relaxation decay.

NMR Spectroscopy and Structure Calculation. For NMR data collection, the sample was dissolved in buffer containing 20 mM deuterated sodium acetate, 1 mM DSS, 1 mM sodium azide, 90% H_2O/10% D_2O, or 99.90% D_2O and adjusted to pH 5.0. The IP-10 concentration used was 2.0 mM.

NMR spectra were collected on the NANUC Varian Inova 800 MHz spectrometer at 30 and 40 °C. NMR data were processed using nmrPipe (*25*) software, and spectral analysis was assisted using the program NMRView (*26*). Assignment of IP-10 proton resonances was achieved using homonuclear NOESY (mixing time 120 ms) and TOCSY (mixing time 44 ms) spectra. $^3J_{NH-H\alpha}$ coupling was quantified using a DQ-COSY. NOEs were assigned using two NOESY experiments (mixing time 120 ms), one in H_2O and one in D_2O.

Structure calculations were performed using version 3.851 of XPLOR with ambiguous restraints for iterative assignment (ARIA) (*27*). The initial input for ARIA consisted of the eight lowest-energy structures calculated by XPLOR using 403 unambiguous manually assigned NOEs, 75 dihedral angle restraints, and 42 hydrogen bond restraints. The dihedral angle restraints were derived from the measured $^3J_{NH-H\alpha}$ coupling constants ($8 < J < 9$, $\phi = -120 \pm 40°$; $J > 9$, $\phi = -120 \pm 30°$), where possible, with the addition of restraints ($\phi = -120 \pm 30°$, $\psi = 120 \pm 40°$ for β-strands; $\phi = -60 \pm 30°$, $\psi = 120 \pm 40°$ for α-helix) where the secondary structure was clearly indicated by NOE patterns, H_α chemical shift values, and lower rates of amide hydrogen exchange. Using these criteria, residues 26−31, 39−45, and 50−54 were judged to be β-strand and residues 59−69 α-helical. Hydrogen bond restraints (H···O, 2.5 Å; N···O, 3.5 Å) were added for β-strand residues and α-helical residues.

Table 1: Structural Statistics for the Ensemble of 10 Calculated Structures[a]

experimental restraints	
NOE restraints (total)	1237
unambiguous (total)	1040
intraresidue	357
sequential	269
medium-range (*i*,*i*+2,3,4)	154
long-range (≥*i*,*i*+5)	260
ambiguous	153
hydrogen bond restraints	42
disulfide bond restraints	2
dihedral angle restraints	75
deviations from experimental restraints (kcal /mol)	
unambiguous NOE restraints	30 ± 9
ambiguous NOE restraints	32 ± 7
dihedral angle restraints	630 ± 110
hydrogen bond restraints	89 ± 3
RMSD from the average structure (residues 7−70)	
backbone	0.50 Å
heavy atoms	1.07 Å
number of residues in most favored region of Ramachandran plot (residues 7−70)	73%

[a] There were no NOE violations greater than 0.3 Å and no dihedral angle violations greater than 5°.

The NOESY spectra in H_2O and D_2O were manually peak picked using NMRView (*26*). The resulting NOE peak lists were used as input for ARIA calculations, along with dihedral and hydrogen bond restraints, as discussed above. The frequency window tolerance for assigning NOEs with ARIA was ±0.015 ppm. The ARIA parameters p, Tv and Nv were the same as those in Nilges et al. (*27*). In each iteration, 20 structures were refined, and the seven lowest-energy structures were used for the purposes of NOE assignments. The hand-assigned NOEs used to calculate the starting structures were retained until the end of the 6th iteration, at which time they were removed in order to allow ARIA calibration of the distance restraints for these NOEs. In the final (eighth) ARIA iteration, 20 structures were refined, and the 10 lowest-energy structures were retained for analysis. A total of 1040 unambiguous and 153 ambiguous NOE-based distance restraints were used for the final set of structures. A summary of the structural statistics is presented in Table 1. The restraints and coordinates for the 10 lowest-energy structures of IP-10 have been deposited in the PDB data bank (1LV9) and the ^{1}H resonance assignments in the BMRB data bank (5383).

CXCR3 Peptide Titration. A peptide consisting of residues 22−42 of human CXCR3, with the nonconserved cysteines 37 and 38 mutated to serine, was titrated into the IP-10 sample used for structure determination. Natural abundance 2D ^{15}N−^{1}H HSQC NMR spectra (*28*) were acquired at CXCR3 peptide to IP-10 ratios of 0:1, 0.1:1, 0.3:1, 0.5:1, 0.75:1, and 1:1. The HSQC spectra were collected at 30 °C

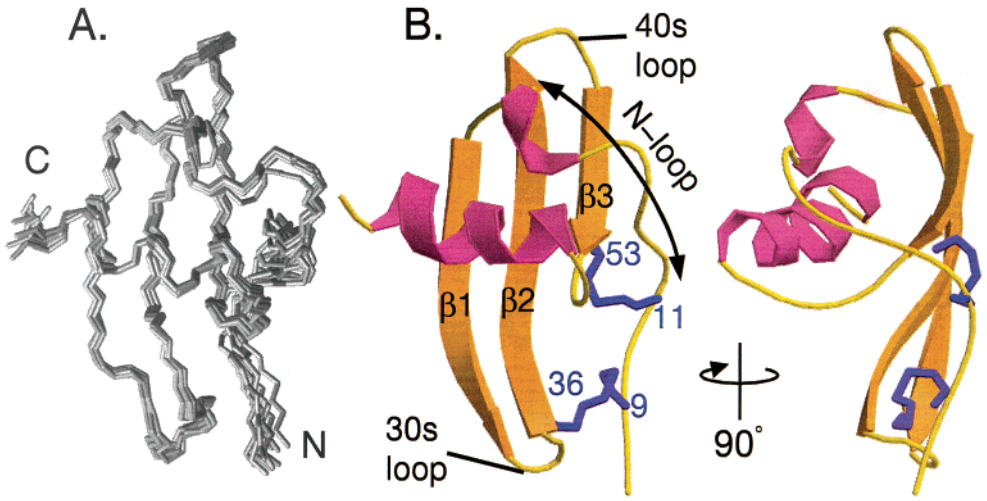

FIGURE 1: NMR structure of IP-10 (residues 7−70). (A) Ensemble of 10 lowest-energy calculated structures (prepared using MOLMOL, *44*). (B) Two views of a ribbon representation of IP-10 (rendered with MOLSCRIPT, *45*). The disulfide bonds are displayed in blue.

on a Varian Unity 600 MHz spectrometer with identical buffer conditions to those used for structure determination. The number of transients used was between 848 and 1216, and the number of nitrogen increments was 100. For well-resolved HSQC peaks, frequency assignment was attained using the amide proton chemical shifts determined in the course of the structure determination. For less well-resolved peaks that experienced changes upon CXCR3 peptide addition, peak assignment was aided by identifying the HSQC peak with a set of peaks in the 2D NOESY that were similarly modified by addition of CXCR3 peptide (at 0.5:1 CXCR3 peptide to IP-10). Peak intensities were normalized using the intensity of 14 peaks that varied the least from experiment to experiment. The intensity of each peak was plotted versus the CXCR3 concentration and fitted with a linear, least-squares routine in order to quantify the change in intensity upon CXCR3 addition.

RESULTS

Structure of IP-10. The majority of chemokines studied have been observed to form dimers at mM concentrations (*11*). Preliminary NMR data obtained for IP-10 indicated that IP-10 also dimerizes. This was judged by the short ^{1}H transverse relaxation rates (average $T_2 = 21$ ms at 30 °C, corresponding to an apparent molecular weight of about 20 kDa; *29*). Sedimentation equilibrium measurements also indicated that IP-10 exists primarily as a dimer (data not shown). Due to the broadness of the spectral lines stemming from the large molecular weight of the dimers, it was possible to obtain only partial NMR resonance assignments for the backbone (residues 6−11, 23−37, 39−53) using wild-type IP-10. In analogy with past work on interleukin-8 (*30*), we disrupted the dimer interface by replacing the amide proton of leucine 27 with a methyl group. The quality of the spectra improved significantly (average $T_2 = 35$ ms at 30 °C, corresponding to an apparent molecular weight of about 11 kDa; *29*), indicating that the mutant exists mainly as a monomer and it was possible to assign all of the ^{1}H NMR resonances corresponding to residues 6−69. No significant difference was observed between the assigned backbone chemical shifts of the IP-10 mutant and those of wild type IP-10. Thus, the introduction of the methyl group does not appear to significantly alter the structure of IP-10, other than to disrupt the dimerization interaction. The structure presented herein is derived from the data acquired with this IP-10 mutant (NMeLeu27).

The structure of IP-10 represents the first from the class of chemokines that bind the receptor CXCR3. IP-10 presents a typical chemokine framework, consisting of a series of loops and one turn of a 3−10 helix at the N-terminus, followed by three antiparallel β strands packed against a C-terminal α-helix (Figure 1). Two pairs of conserved cysteines, 9−36 and 11−53, form disulfide bonds. Residues 1−6 and 70−77 do not form a defined structure. Residues 12 and 13 exhibit no long range NOEs and appear to be tethered between more structured regions of the backbone, rather than interacting directly with the rest of the protein.

A feature of the IP-10 structure that appears unusual, in comparison to most other chemokines, is the distortion of β-strand 2 that leads to closer contact between the sheet and the helix (Figure 2). To confirm the conformation of the distortion, structures were recalculated after removing various subsets of NOE distance restraints involving this region. The distortion only disappeared after virtually all the restraints for this region were removed, confirming that this conformation was not caused by a small subset of distance restraints that may have been incorrect. This structural feature is shared with the CC chemokine eotaxin-2 and may provide a structural basis for the ability of IP-10 to interact with the CC receptor, CCR3, as detailed in the discussion.

Binding to CXCR3. To investigate which regions of IP-10 are involved in binding to the receptor, a peptide of the N-terminus of CXCR3 was designed, based on the region of CXCR1 shown to bind IL-8 (*31*). The peptide consisted of residues 22−42 of CXCR3, with nonconserved cysteines 37 and 38 replaced by serines.

The CXCR3 peptide was titrated into the IP-10 sample, and changes in natural abundance 2D ^{15}N−^{1}H HSQC, 1D proton, and 2D homonuclear NOESY NMR spectra of IP-10 were followed. Significant reductions in cross-peak intensity in the HSQC spectra were noted for residues 7, 8, 17, 19, 38, and 44 upon addition of CXCR3 (Figure 3). For some peaks, the loss in intensity was associated with the appearance of a new HSQC peak nearby (e.g., residues 7

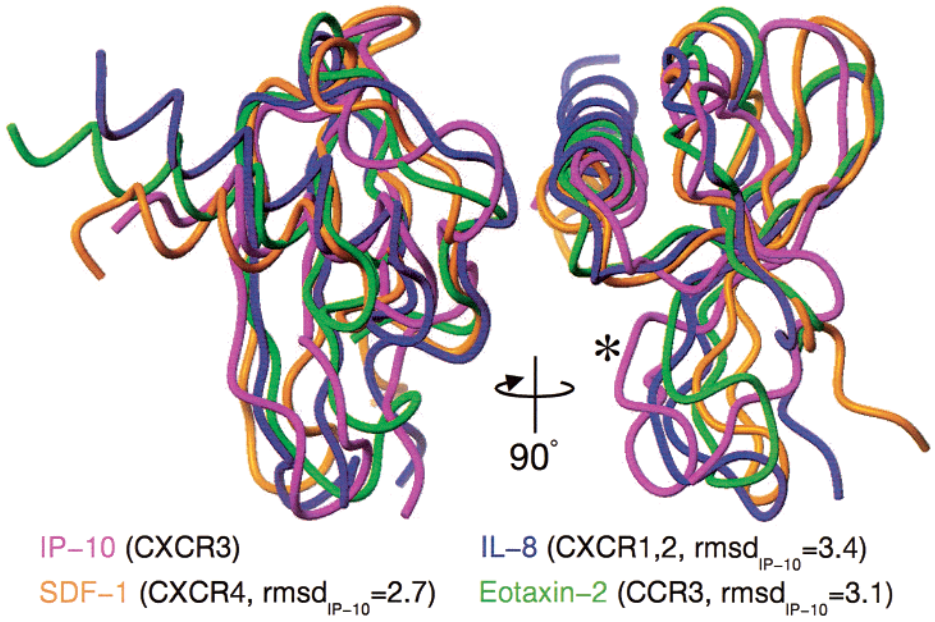

FIGURE 2: Comparison of IP-10 with other chemokines. Coil representations of IP-10 (magenta), IL-8 (blue, 1IKL, *30*), SDF-1 (orange, 1A15, *37*), and eotaxin-2 (green, 1EIH, *39*). IL-8, SDF-1, and eotaxin-2 were aligned to IP-10 according to the optimal alignment as determined by DALI (*36*) (IL8, residues 7−17, 20−34, 38−44, 45−67; IP10, 9−19, 22−36, 40−46, 48−70; SDF-1, 9−17,1 8−29, 30−36, 37−53, 54−57, 58−63; IP10, 9−17, 19−30, 32−38, 40−56, 60−63, 65−70; Eotaxin-2, 7−14, 15−18, 21−27, 28−32, 36−42, 43−52, 53−62; IP10, 10−17, 20−23, 24−30, 32−36, 40−46, 48−57, 61−70). The receptor for each chemokine and backbone RMSD (Å) when fit to IP-10 is indicated in brackets on the figure legend. For clarity, the extreme N-termini are not shown. An asterix (*) indicates the distortion in the β-strand 2 of IP-10.

and 44), representing the bound chemical shift of the resonance. For residue 19, it was possible to track the shift in frequency as CXCR3 peptide was bound. Because of the low signal-to-noise in the natural abundance $^{15}N-^{1}H$ HSQC spectra, quantitative changes in peak intensity and position are best indicated by the least-squares fit of the $^{15}N-^{1}H$ HSQC peak intensity versus the CXCR3 peptide concentration shown inTable 2, rather than from visual inspection of the representative countour plots shown in Figure 3.

At first glance, it might seem that having some peaks disappear and reappear at a new chemical shift, and other peaks just shifting in position, would indicate that some of the peaks are undergoing exchange on a slow to intermediate time scale and some on a fast time scale. Line shape simulations (see supplementary data) show that the behavior of all the peaks can be accounted for using a single dissociation rate. The apparently disparate behavior of the peaks arises from the dependence of the line shape on the chemical shift difference between the bound and unbound states. Larger chemical shift differences lead to the appearance of a new peak concommitently with loss of intensity at the original frequency (for example, peak 7), and smaller chemical shift differences give rise to a gradual shifting and broadening of the peak (for example, peak 19). Simulations (*32*) using an off rate of 20 s^{-1} fit the line shapes observed. Assuming an on rate of 10^7 M^{-1} s^{-1} (close to the diffusion limit) leads to a dissociation constant of $\sim$ 2 μM. This implies tighter binding than has been observed for other chemokine/receptor peptide interactions, K_d $\sim$100 μM (*31*, *38*).

It is interesting to note that in the case of residue 44, there is a small peak present in the spectrum of IP-10 alone, at the position of the new peak. These may indicate that, for a small fraction of the free IP-10, residue 44 takes on the same conformation that it does in the receptor peptide bound state, but given the low signal-to-noise in the natural abundance HSQC spectra, no definitive conclusion can be drawn.

DISCUSSION

Numerous studies with chemokine and receptor mutants (*2*, *33*−*35*) have shown that receptor binding and activation can be dissociated and the process can be described by a "two-step" model. In the first step, the chemokine binds to a region on the N-terminus of the receptor. In the second step, residues on the N-terminus of the chemokine bind to a second site on the receptor and effect the switch of the receptor to the active form. The critical region of the chemokine for step 1, the "docking domain", is the region between the first pair of conserved cysteines and the first β-strand, called the N-loop, which contributes to binding and is responsible for receptor recognition. The activation step is attributed to the unstructured N-terminus of the chemokine, or the "triggering domain". Mutations in this region severely affect receptor activation with more modest effects on binding.

Although it maintains a typical chemokine framework, there are significant differences between the structure of IP-10 and other chemokines. IP-10 was compared with other chemokine structures using the program DALI (*36*) to determine the optimal segments over which to perform backbone alignments. For clarity, only three comparison structures are displayed with IP-10 in Figure 2. Overall, the backbone trace of IP-10 follows most closely that of SDF-1 (*37*) (RMSD 2.7 Å), especially in the placement of the α-helix and the positioning of the loop between strands 2 and 3 (40s-loop), which, together with the N-loop region, have been shown to be critical for receptor binding. SDF-1 binds the receptor CXCR4 and is one of the closer sequence

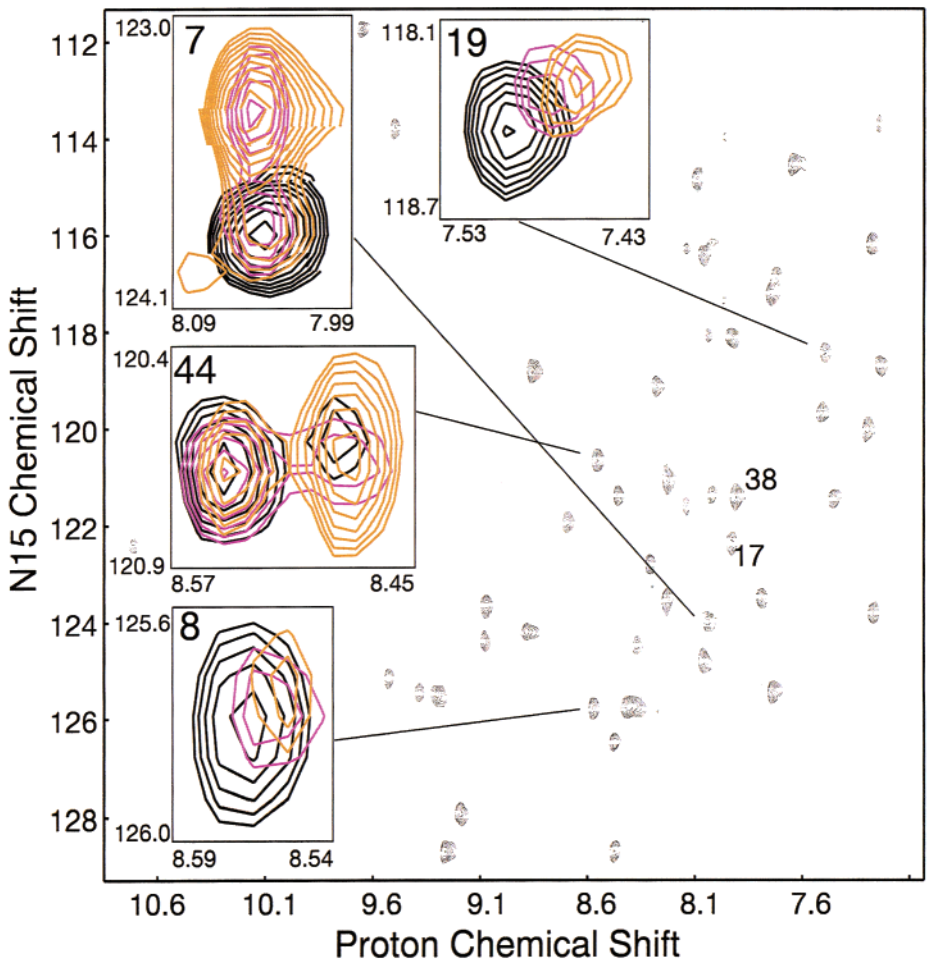

FIGURE 3: Natural abundance $^{15}N-^{1}H$ HSQC of IP-10 (black), 0.5:1 CXCR3 peptide:IP-10 (magenta), and 1:1 CXCR3 peptide:IP-10 (orange). Residues exhibiting changes upon CXCR3 peptide addition are labeled, and a subset of these is shown in greater detail in the insets. For clarity, the spectra of IP-10 with CXCR3 peptide added are shown only in the insets.

Table 2: Summary of the Changes in IP-10 $^{15}N-^{1}H$ HSQC Peak Intensity and Frequency Induced by the CXCR3 Peptide[a]

residue	percent intensity change[b] at 1:1 CXCR3:IP10	frequency shift at 1:1 CXCR3:IP10
V7	$-63 \pm 5\%$	–
R8	$-38 \pm 10\%$	–
Q17	$-46 \pm 13\%$	–
V19	–	N^{15}: -0.21 ± 0.02 ppm H^{1}: -0.044 ± 0.006 ppm
Q34	$-23 \pm 10\%$	–
R38	$-81 \pm 21\%$	–
T44	$-26 \pm 11\%$	–

[a] Only the data for peaks with significant changes are shown. [b] The percent change in IP-10 HSQC peak intensity induced by the addition of 1:1 CXCR3 peptide, determined using a linear least-squares fit of the peak intensity at six peptide concentrations (ranging from 0:1 CXCR3:IP-10 to 1:1 CXCR3:IP-10).

neighbors (27% identity) to IP-10. Even though there is greater sequence similarity between IP-10 and IL-8 (22% identity), the structure of IP-10 appears less similar to IL-8 (*30*) (RMSD 3.4 Å) than to SDF-1. Interestingly, a chimera consisting of the N-terminal 17 residues of SDF-1 and the C-terminus of IP-10 retains SDF-1-like activation (*38*). However, a similar chimera using SDF-1 and IL-8 was completely inactive, perhaps indicating a closer structural, and hence functional, relationship between IP-10 and SDF-1 than between these chemokines and IL-8.

When compared to most other chemokines, one feature of IP-10 that seems unusual is the distortion of strand 2 of the β-sheet that causes the sheet to curve toward the α-helix (marked by an asterix in Figure 2). Interestingly, a chemokine from the CC class of chemokines, eotaxin-2, has a similar structural feature (*39*). This is consistent with the observation that both eotaxin-2 and IP-10 bind the same receptor, CCR3 (*7*), although eotaxin-2 binds as an agonist and IP-10 as an antagonist. However, the structure of the related chemokine eotaxin-1, which also binds CCR3, does not exhibit this feature.

Inspection of the hydrophobic cores of several chemokines (Figure 4 reveals that in IP-10 and eotaxin-2, hydrophobic residues from the α-helix pack against residues from the "lower" (more proximal to the 30s-loop) region of the β-sheet. These core interactions are not observed in IL-8 and SDF-1, or in any other of the several chemokines inspected, and result in the β-sheet being angled up toward the α-helix to a greater extent in IP-10 and eotaxin-2 than in other chemokines.

Modification of the position of strands 1 and 2 has ramifications for the placement and functioning of the 30s-loop that joins them. The 30s-loop of eotaxin-1 has been shown to exhibit motion on a slow (microsecond to millisecond) time scale (*40*) and has been implicated in receptor binding and/or activity for IL-8, eotaxin, and MCP-1 (*33*,

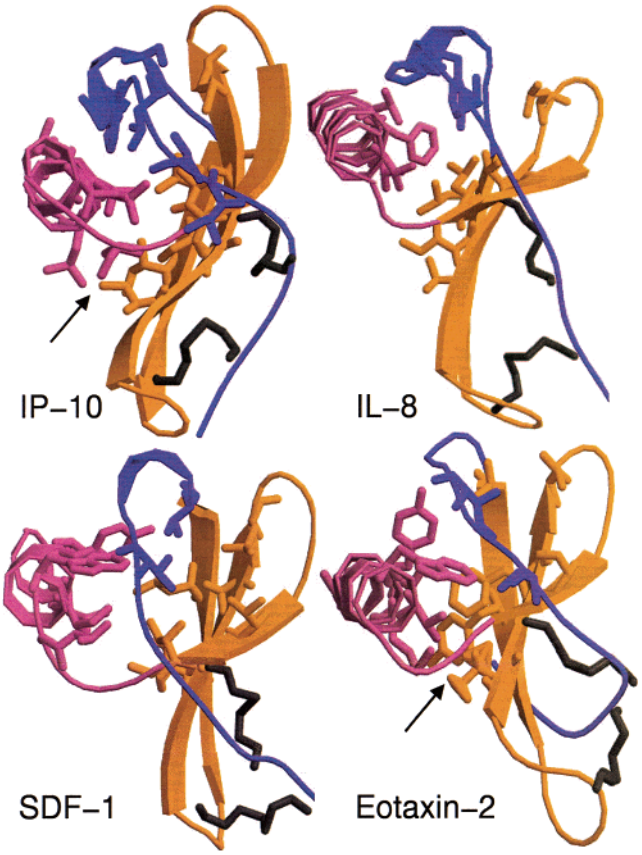

FIGURE 4: Hydrophobic core of IP-10, SDF-1, IL-8, and eotaxin-2 (rendered using MOLSCRIPT, *45*). Only IP-10 and eotaxin-2 have hydrophobic residues from the helix that pack against the "lower" region of the sheet formed by the C-terminal region of strand 1 and the N-terminal region of strand 2 (indicated by arrows).

40, *41*). A study of concerted motions in the chemokine family (*42*) classified chemokines into two groups based on how the three flexible regions of chemokines shown to be important in receptor interactions, the N-terminus, the N-loop, and the 30s-loop, correlate with respect to their motions. All the CXC chemokines studied were found to have positive correlations between the motions of the 30s-loop and the N-terminus. Most CC chemokines possessed correlations between the 30s-loop and the N-loop, except for eotaxin and HCC-2, which exhibited CXC-like correlations. This finding, along with the observed structural similarities between IP-10 and eotaxin-2 and the fact that IP-10 and the eotaxins all interact with the chemokine receptor CCR3, points to similarities in the mechanism, involving the 30s-loop, by which these chemokines interact with their receptors.

The positioning of the N-terminal region of chemokines proximal to the two N-terminal conserved cysteines is highly variable. As seen in Figure 3, IP-10 is no exception to this rule. This variability is in keeping with the apparent role for this region in determining receptor specificity (*2*, *33*−*35*).

In the second part of this study, the changes in chemical shift (resonance frequency) of IP-10 backbone amides induced by binding a receptor N-terminal peptide were used to probe the nature of the IP-10/receptor interaction. Chemical shift depends on the chemical environment surrounding a nucleus and is thus a sensitive probe for local changes in structure. Seven IP-10 $^{15}N-^{1}H$ HSQC peaks were found to undergo changes in intensity or position with addition of CXCR3 receptor peptide. Two of these residues are located just N-terminal to the first two conserved cysteines, two on the N-loop region, one on the 30s-loop between β-strands 2 and 3, and two on β-strand 2 (Figure 5A).

The overall distribution of residues found to be affected by the addition of receptor peptide agrees well with the results of similar studies using IL-8 (*31*), fractalkine (*43*), and especially eotaxin-2 (*39*), where line-shape changes were observed for residues in the N-terminal region from residue 5 to 16 and in 30s-loop/β-strand 2 residues 34−37. Five out of seven of the IP-10 residues affected by CXCR3 binding map to one face of the protein (Figure 5C). This face contains a hydrophobic cleft, formed by the N-loop and 40s-loop, similar in character to the region of IL-8 that contacts the receptor peptide in the NMR structure of an IL-8 receptor peptide complex (*31*). However, IP-10 possesses an additional hydrophobic cleft between the N-terminal residues and the 30s-loop. Three of the IP-10 residues that exhibited spectral changes upon addition of CXCR3, V7, R8, and R38 contribute to this cleft, indicating that IP-10 may also use this region to bind the receptor.

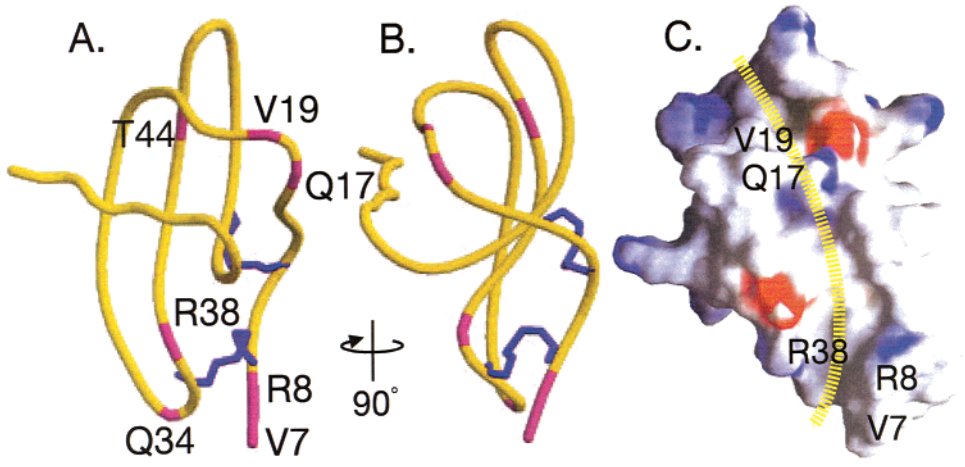

FIGURE 5: IP-10 residues that experienced changes in $^{15}N-^{1}H$ HSQC peak intensity or position upon addition of CXCR3 peptide. (A) Ribbon plot of IP-10. (B) View A rotated clockwise, 90°. (C) Electrostatic surface plot (same orientation as panel B). The path the receptor peptide may take across IP-10 is indicated by the dashed yellow line. Panels A and B were produced using MOLSCRIPT (*45*) and C with GRASP (*46*).

With chemokines that bind neutrophils, including IL-8, the three residues N-terminal to the first conserved cysteine form a highly conserved motif, "ELR". The CXCR3 binding chemokines do not contain this motif, although they do retain the conserved R immediately N-terminal to the first cysteine. The ELR motif is extremely sensitive to modification, as mutations in any one of these residues leads to significant reduction in binding affinity and activity of the chemokine (*34*). There are mutations in this region that completely abrogate function but only reduce binding affinity, in agreement with a two-step model where the ELR motif is responsible for the second step of chemokine-receptor interaction, binding to the transmembrane portion of the receptor. In contrast to IL-8, the conserved R, as well as the adjacent V, of IP-10 experience changes in chemical shift upon binding to CXCR3 peptide. This indicates that these N-terminal residues of IP-10 likely contribute to binding the N-terminus of the receptor, rather than the transmembrane region of the receptor.

The N-loop region, between the second conserved cysteine and the first β-strand, has been shown to be critical in chemokine receptor recognition and binding (*2*, *33*−*35*). In keeping with this, the amide resonance frequencies of Q17 and V19 of IP-10 were altered by addition of receptor peptide. These residues are located in a hydrophobic cleft between the N-loop and the 40s-loop, a region of IP-10's surface very similar in character to the region of IL-8 that has been shown to bind a CXCR1 N-terminal peptide (*31*).

The remaining IP-10 residues affected by binding of the receptor peptide are on β-strand 2 and the loop between strands 1 and 2. Q34 is located in the 30s-loop which has, as discussed above, been identified as one of the flexible regions of chemokines involved in activity. R38 maps to the same face of IP-10 as the N-terminal and N-loop residues involved in receptor binding (Figure 5). The involvement of residue T44 is not obvious because it is not located on the same surface of IP-10 as the other residues. It is a buried residue, located close to the 40s-loop between strands 2 and 3 that forms part of the hydrophobic cleft and so could be affected by a change in conformation in this area.

In conclusion, this study provides the first structure of a CXCR3 binding chemokine. The structure of IP-10 provides some physical basis for the observed ability of these chemokines to act as antagonists for CCR3, in that there are similarities in the configuration of β-strand 2 and the 30s-loop between IP-10 and the CCR3 agonist, eotaxin-2. Additionally, we defined the region of IP-10 that interacts with the N-terminus of CXCR3. This region is similar overall to what has been observed in other chemokines, but there are some details of the interaction which appear to differ from the most intensively investigated CXC chemokine, IL-8. Residues N-terminal to the first conserved cysteine of IP-10 were observed to contribute to binding the N-terminus of the receptor, in contrast to IL-8, where these residues appear to interact with the main body of the receptor and not the N-terminus.

ACKNOWLEDGMENT

We are grateful for the assistance of Les Hicks with the sedimentation equilibrium studies.

REFERENCES

1. Mackay, C. (2001) *Nature Immun. 2*, 95−101.
2. Fernandez, E. J., and Lolis, E. (2002) *Annu. Rev. Pharmacol. Toxicol. 42*, 469−99.
3. Rojo, D., Suetomi, K., and Navarro, J. (1999) *Biol. Res. 32*, 263−272.
4. Power, C., and Proudfoot, A. (2001) *Curr. Opin. Pharm. 1*, 417−424.
5. Loetscher, M., Loetscher, P., Brass, N., Meese, E., and Moser, B. (1998) *Eur. J. Immunol. 28*, 3696−3705.
6. Jenh, C., Cox, M., Hipkin, W., Lu, T., Pugliese-Sivo, C., Gonsiorek, W., Chou, C., Narula, S., and Zavodny, P. (2001) *Cytokine 15*, 113−121.
7. Loetscher, P., Pellegrino, A., Gong, J. H., Mattioli, I., Loetscher, M., Bardi, G., Baggiolini, M., and Clark-Lewis, I. (2001) *J. Biol. Chem. 276*, 2986−91.
8. Horuk, R. (2001) *Cytokine Growth Factor Rev. 12*, 313−35.
9. Luster, A., Unkeless, J., and Ravetch, J. (1985) *Nature 315*, 672−676.
10. Liao, F., Rabin, R., Yannelli, J., Koniaris, L., Vanguri, P., and Farber, J. (1995) *J. Exp. Med. 182*, 1301−14.
11. Baggiolini, M. (1997) *Annu. Rev. Immun. 15*, 675−705.
12. Flier, J., Boorsma, D., van Beek, P., Nieboer, C., Stoof, T., Willemze, R., and Tensen, C. (2001) *J. Pathol. 194*, 398−405.
13. Balashov, K., Rottman, J., Weiner, H., and Hancock, W. (1999) *Proc. Natl. Acad. Sci. U.S.A. 96*, 6873−6878.
14. Sorensen, T., Tani, M., Jensen, J., Pierce, V., Lucchinetti, C., Folcik, V., Qin, S., Rottman, J., Sellebjerg, F., Strieter, R., Frederiksen, J., and Ransohoff, R. (1999) *J. Clin. Invest. 103*, 807−815.
15. Angiolillo, A., Sgadari, C., Taub, D., Liao, F., Farber, J., Maheshwari, S., Kleinman, H., Reaman, G., and Tosato, G. (1995) *J. Exp. Med. 182*, 155−162.
16. Strieter, R., Polverini, P., Kunkel, S., Arenberg, D., Burdick, M., Kasper, J., Dzuiba, J., Van Damme, J., Walz, A., Marriott, D., and Kunkel, S. (1995) *J. Biol. Chem. 270*, 27348−57.
17. Hancock, W., Gao, W., Csizmadia, V., Faia, K., Shemmeri, N., and Luster, A. (2001) *J. Exp. Med. 193*, 975−980.
18. Romagnani, P., Annunziato, F., Lazzeri, E., Cosmi, L., Beltrame, C., Lasagni, L., Galli, G., Francalanci, M., Manetti, R., Marra, F., Vanini, V., Maggi, E., and Romagnani, S. (2001) *Blood 97*, 601−607.
19. Meyer, M., Hensbergen, P., van der Raaij-Helmer, E., Brandacher, G., Margreiter, R., Heufler, C., Koch, F., Narumi, S., Werner, E., Colvin, R., Luster, A., Tensen, C., and Werner-Felmayer, G. (2001) *Eur. J. Immunol. 31*, 2521−2527.
20. Cole, K., Strick, C., Paradis, T., Ogborne, K., Loetscher, M., Gladue, R., Lin, W., Boyd, J., Moser, B., Wood, D., Sahagan, B., and Neote, K. (1998) *J. Exp. Med. 187*, 2009−2021.
21. Clark-Lewis, I., Vo, L., Owen, P., and Anderson, J. (1997) *Methods Enzymol. 287*, 233−250.
22. Rajarathnam, K., Sykes, B. D., Kay, C. M., Geiser, T., Dewald, B., Baggiolini, M., and Clark-Lewis, I. (1994) *Science 264*, 90−92.
23. Gueron, M., Plateau, P., and Kettani, A. (1992) *J. Magn. Reson. 96*, 541−550.
24. Plateau, P., and Gueron, M. (1982) *J. Am. Chem. Soc. 104*, 7310−7311.
25. Delaglio, F., Grzesiek, S., Vuister, G. W., Zhu, G., Pfeifer, J., and Bax, A. (1995) *J. Biomol. NMR 6*, 277−93.
26. Johnson, B., and Blevins, R. (1994) *J. Biomol. NMR 4*, 603−614.
27. Nilges, M., Macias, M., O'Donoghue, S., and Oschkinat, H. (1997) *J. Mol. Biol. 269*, 408−422.
28. Bax, A., Clore, G., and Gronenborn, A. (1990) *J. Magn. Res. 88*, 425−341.
29. Anglister, J., Ren, H., Klee, C., and Bax, A. (1993) *J. Biol. NMR 3*, 121−126.
30. Rajarathnam, K., Clark-Lewis, I., and Sykes, B. (1995) *Biochemistry 34*, 12983−90.
31. Skelton, N., Quan, C., Reilly, D., and Lowman, H. (1998) *Structure Fold. Des. 7*, 157−168.
32. Li, M., Saude, E., Wang, X., Pearlstone, J., Smillie, L., and Sykes, B. (2002) *Eur. Biophys. J.* (in press).
33. Clark-Lewis, I., Dewald, B., Loetscher, M., Moser, B., and Baggiolini, M. (1994) *J. Biol. Chem. 269*, 16075-1081.

34. Clark-Lewis, I., Kim, K., Rajarathnam, K., Gong, J., Dewald, B., Moser, B., Baggiolini, M., and Sykes, B. (1995) *J. Leukoc. Biol. 57*, 703−711.
35. Baggiolini, M. (2001) *J. Intern. Med. 250*, 91−104.
36. Holm, L., and Sander, C. (1993) *J. Mol. Biol. 233*, 123−138.
37. Dealwis, C., Fernandez, E., Thompson, D., Simon, R., Siani, M., and Lolis, E. (1998) *Proc. Natl. Acad. Sci. U.S.A. 95*, 6941−6946.
38. Crump, M., Gong, J., Loetscher, P., Rajarathnam, K., Amara, A., Arenzana-Seisdedos, F., Virelizier, J., Baggiolini, M., Sykes, B., and Clark-Lewis, I. (1997) *EMBO J. 16*, 6966−7007.
39. Mayer, K. L., and Stone, M. J. (2000) *Biochemistry 39*, 8382−95.
40. Crump, M. P., Spyracopoulos, L., Lavigne, P., Kim, K. S., Clark-lewis, I., and Sykes, B. D. (1999) *Protein Sci. 8*, 2041−54.
41. Hemmerich, S., Paavola, C., Bloom, A., Bhakta, S., Freedman, R., Grunberger, D., Krstenansky, J., Lee, S., McCarley, D., Mulkins, M., Wong, B., Pease, J., Mizoue, L., Mirzadegan, T., Polsky, I., Thompson, K., Handel, T., and Jarnagin, K. (1999) *Biochemistry 38*, 13013−13025.
42. Baysal, C., and Atilgan, A. (2001) *Proteins 43*, 150−160.
43. Mizoue, L., Bazan, J., Johnson, E., and Handel, T. (1999) *Biochemistry 38*, 1402−1414.
44. Koradi, R., Billeter, M., and Wuthrich, K. (1996) *J. Mol. Graphics 14*, 51−55.
45. Kraulis, P. (1991) *J. Appl. Crystallogr. 24*, 946−950.
46. Nicholls, A., Sharp, K., and Honig, B. (1991) *Proteins: Struct., Funct., Genet. 11*, 281.

BI026020Q